Hindawi Publishing Corporation
International Journal of Antennas and Propagation
Volume 2014, Article ID 173704, 11 pages
http://dx.doi.org/10.1155/2014/173704

Research Article

Two-Step Beveled UWB Printed Monopole Antenna with Band Notch

Yan Xiao,[1] Zhong-Yong Wang,[1] Ji Li,[2] Zi-Lun Yuan,[2] and A. K. Qin[3]

[1] *The Institute of Information Engineering, Zhengzhou University, Zhengzhou, Henan 450000, China*
[2] *Department of Wireless Communication, Zhengzhou Locaris Electronics Technology Co., Ltd, Zhengzhou, Henan 450000, China*
[3] *School of Computer Science and Information Technology, RMIT University, Melbourne, VIC 3001, Australia*

Correspondence should be addressed to Zhong-Yong Wang; iezywang@zzu.edu.cn

Received 1 January 2014; Revised 27 March 2014; Accepted 24 April 2014; Published 27 May 2014

Academic Editor: Renato Cicchetti

Copyright © 2014 Yan Xiao et al. This is an open access article distributed under the Creative Commons Attribution License, which permits unrestricted use, distribution, and reproduction in any medium, provided the original work is properly cited.

This paper presents a novel compact printed monopole ultra-wideband (UWB) antenna featured with the band notch. The proposed antenna consists of a two-step beveled radiant patch and a truncated ground plane, which can provide a good impedance matching from 3.1 GHz to 10.6 GHz. In order to generate the band-notched characteristics, two symmetrical slots are embedded along with the microstrip feeding line, resulting in a band notch from 5.05 GHz to 5.85 GHz. Accordingly, the mutual electromagnetic interference between the UWB and wireless local area network (WLAN) radio communication systems can be eliminated. In addition, it is shown how the slots integrated on the ground plane improve the radiation patterns. The experimental measurements are found to be in good agreement with the numerical simulations.

1. Introduction

In 2002, the Federal Communications Commission (FCC) approved the use of the unlicensed band with the frequencies ranging from 3.1 GHz to 10.6 GHz in the commercial ultra-wideband (UWB) wireless communication systems [1]. This invoked a surge in research on the UWB communication technology. Impulse radio UWB (IR-UWB) is a promising UWB communication technique having a simple architecture. In the IR-UWB systems, short duration pulses are usually adopted as exciting signals. However, as a well-known fact, the presence of frequency distortions in the surface current distribution excited on the antenna will give rise to strongly distorted radiated signals. Therefore, to enable the antenna to radiate undistorted pulses, the design of antennas in the UWB systems is subject to the following requirements. Firstly, the impedance band must cover the frequency range from 3.1 GHz to 10.6 GHz. Secondly, the radiation patterns must be uniform over the entire operational band. Recently, the UWB antenna design has received more and more attention.

Thanks to their inherent advantages (e.g., the low cost, the easy integrability with the passive and active components, etc.), various types of printed antennas, such as the printed dipoles [2–4] and the printed monopoles, and the slot antennas [5, 6] have been widely used in the UWB communication systems.

Cappelletti et al. developed an antipodal drop-shaped dipole antenna [2]. This antenna not only can exhibit the good radiation performance in the frequency domain but also demonstrate the excellent signal fidelity in the time domain. It is fabricated on a thin flexible substrate, which can be made conformal easily. Moreover, the authors described a method useful to realize a compact array of antennas. Quintero and Skrivervik produced a dipole antenna that is symmetrical and elliptical [3]. This antenna is differential and can be directly connected to a differential circuit. Teni et al. fabricated an antipodal Vivaldi antenna [4] that operates over a broad frequency range from 5 GHz to 30 GHz. This antenna has the peak gain over 5 dBi and presents stable radiation patterns. As an important class of planar radiators, such dipole antennas have several unique advantages. Firstly, they can reduce the level of the field radiated in the direction of the feeding line where the sensitive electronic circuitry, used to process the radio frequency signal transmitted or received

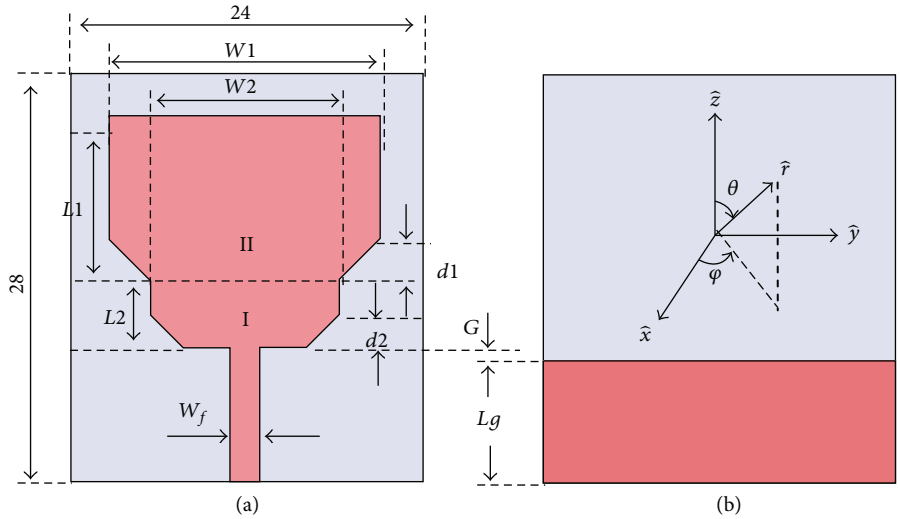

Figure 1: Geometry of the two-step beveled antenna: (a) top view and (b) bottom view.

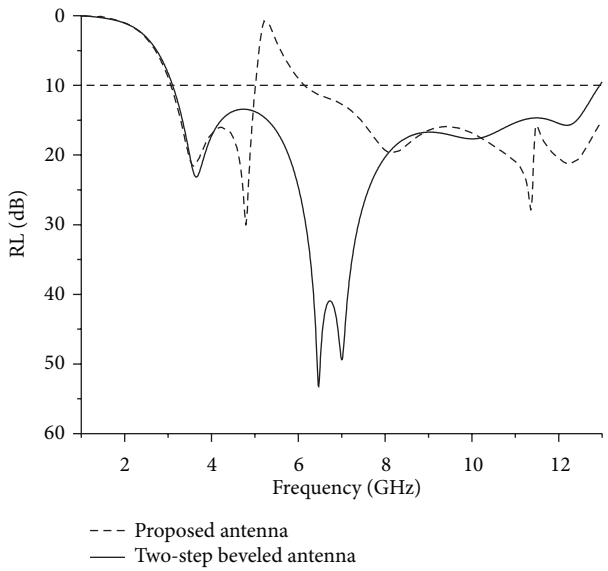

Figure 2: Return loss versus frequency (solid line: the two-step beveled antenna and dash line: the proposed antenna).

by the antenna, is located. Secondly, their symmetrical or antipodal radiating structures allow the generation of the symmetrical and stable radiation patterns. Thirdly, they can be fed in both unbalanced and balanced manners. Finally, they can be adopted to realize the antenna arrays, which ensure the gain enhancement. The UWB antenna arrays have been widely used in various microwave through-wall imaging applications. Despite their advantages, the dipole antennas are almost twice the size of the monopole ones. Therefore, it is more reasonable to use the monopole antennas in the compact devices, such as tags.

However, the printed monopoles, such as those having the rectangular, circular, elliptical, or triangular shape, can hardly guarantee a frequency band from 3.1 GHz up to 10.6 GHz. In recent years, various impedance matching methods, such as the asymmetric feed technology [7, 8], the external π-shaped matching network [9], and the notched ground [10–12], have been proposed to broaden the bandwidth of conventional monopoles. Furthermore, the band overlapping between the UWB and WLAN may induce the mutual electromagnetic interference. Therefore, the antennas for UWB applications must be designed in such a way to limit or even eliminate the electromagnetic interference with the WLAN communication systems. The C-shaped, T-shaped, and dual U-shaped stubs and slots loaded on the radiation patch [9, 10, 13–16], the defected ground structure (DGS) [17], and the electromagnetic band gap (EBG) [18] have been employed to form a band rejection in an expectant frequency band. Although these antennas have a number of practical advantages, they suffer from some limitations such as the large antenna size and the variation of the radiation patterns at higher frequencies. To overcome these limitations, the antennas with the band notch and stable radiation patterns have attracted more and more attention.

This paper presents a novel compact planar two-step beveled UWB antenna. The symmetrical slots integrated on the microstrip line rather than on the radiant patch generate the frequency band notch, while the slots integrated on the ground plane are adopted to improve the radiation patterns. The analysis and design of the proposed antenna have been carried out using 3D full-wave numerical simulation software. The experimental measurements have been shown to be in good agreement with the numerical simulations.

2. Antenna Design

2.1. Design of the Two-Step Beveled Structure. The geometry of the two-step beveled UWB antenna is shown in Figure 1. The dimensions of this antenna, including the low-cost FR4 substrate with the relative dielectric constant of 4.4 and the thickness of 1 mm, are 24 mm × 28 mm. The radiator is printed on the top layer of the substrate, which consists of

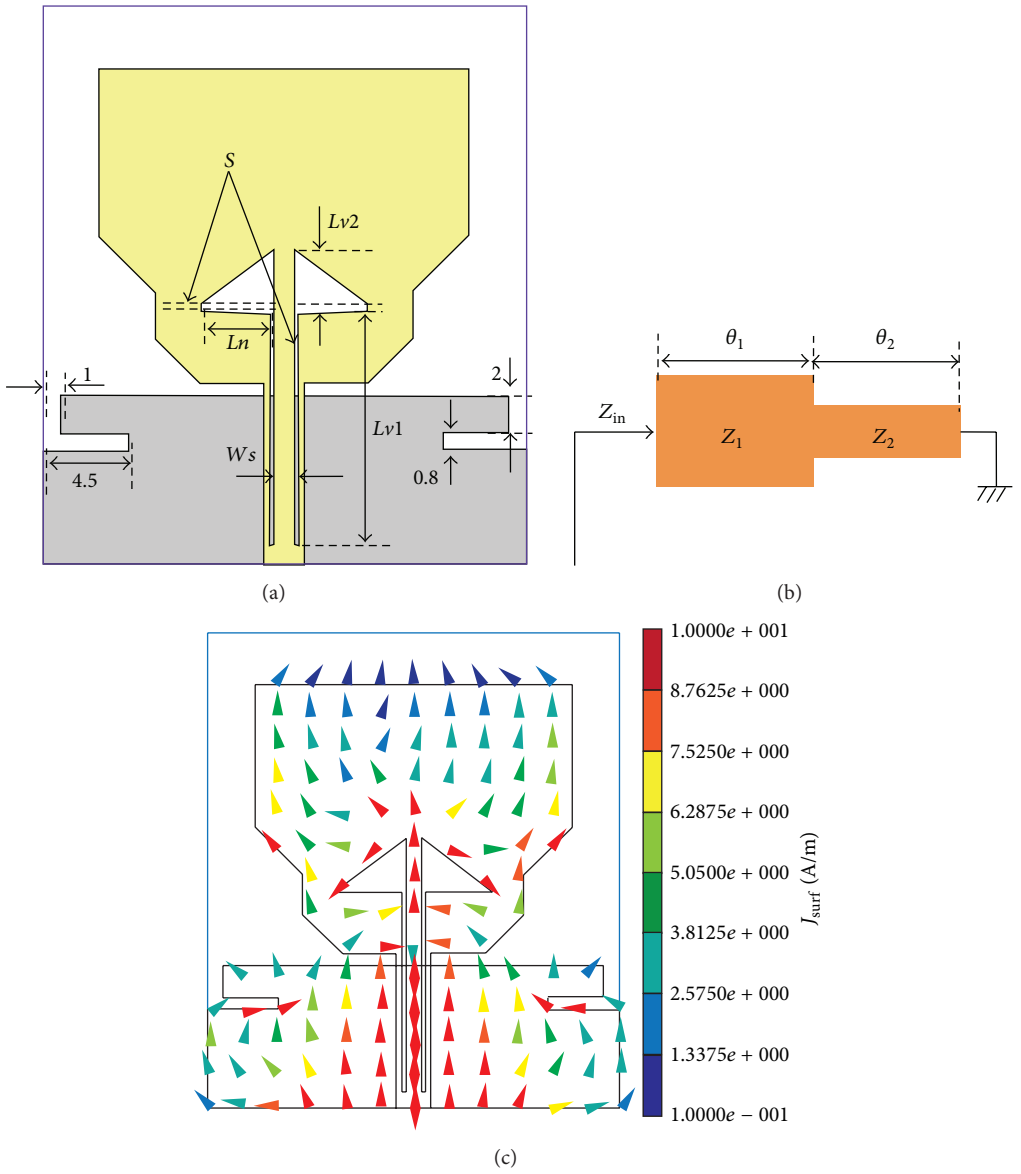

FIGURE 3: The proposed antenna with the band notch: (a) geometry of the proposed antenna, (b) structure of the SIR, and (c) current distribution at 5.5 GHz.

two differently sized rectangular patches with the chamfered corner of 45°. A microstrip line printed on the top layer is used to feed the radiator centrally. To obtain the characteristic impendence of 50 Ω, the width of the microstrip line, as denoted by W_f, in Figure 1(a), is fixed at 2.2 mm. The truncated ground is printed on the backside of the substrate.

This kind of structure can reduce the influence of the discontinuity present in the antenna feeding point, which is achieved by gradually changing the distribution of the current that flows from the feeding line to the radiant patch. In fact, to a certain extent, the smoothness of the current distribution improves the impedance matching. Table 1 reports the parameters of the antenna illustrated in Figure 1. The high frequency structure simulator (HFSS) has been employed to perform the antenna design. The simulation results, as illustrated in Figure 2, indicate that the band with the return loss above 10 dB covers the range from 3 GHz to 13 GHz, and thus the ultra-wideband impedance matching is achieved.

TABLE 1: Parameters of the two-step beveled monopole antenna.

Parameters	Value (mm)	Parameters	Value (mm)
W1	20	*d1*	3
W2	14	*d2*	2.5
L1	11	*G*	0.7
L2	5	*Lg*	9

2.2. Design of the Band-Notched UWB Antenna. According to the standard 802.11a, the frequency band that ranges from

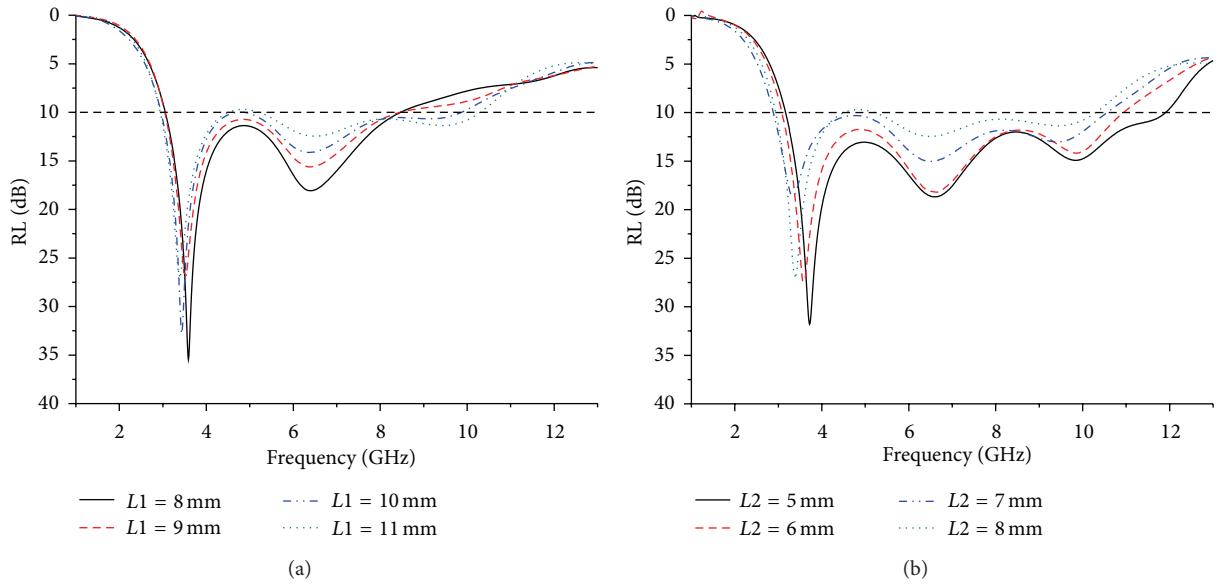

FIGURE 4: Return loss versus frequency (a) for different values of the parameter *L1* (other parameters: $G = 1$ mm, $L2 = 8$ mm, $Lg = 9$ mm, $W2 = 14$ mm, $W1 = 20$ mm, $d1 = 0$, and $d2 = 0$) and (b) for different values of the parameter *L2* (other parameters: $G = 1$ mm, $L2 = 11$ mm, $Lg = 9$ mm, $W2 = 14$ mm, $W1 = 20$ mm, $d1 = 0$, and $d2 = 0$).

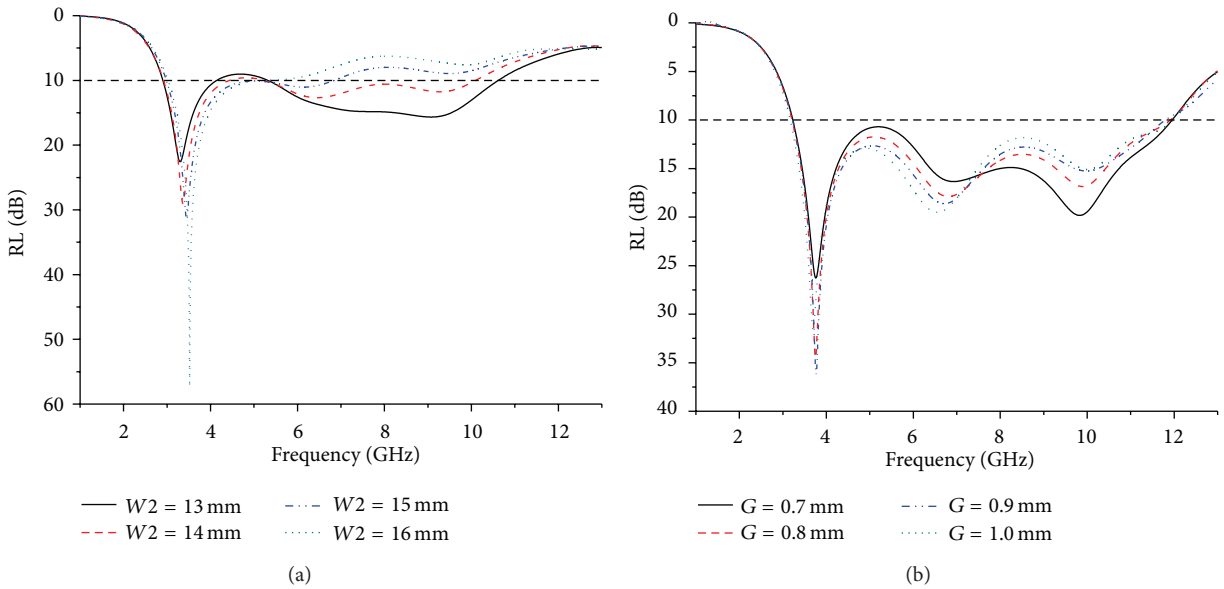

FIGURE 5: Return loss versus frequency (a) for different values of the parameter *W2* (other parameters: $G = 1$ mm, $L2 = 11$ mm, $Lg = 9$ mm, $L2 = 5$ mm, $W1 = 20$ mm, $d1 = 0$, and $d2 = 0$) and (b) for different values of the parameter *G* (other parameters: $W2 = 5$ mm, $L2 = 11$ mm, $Lg = 9$ mm, $L2 = 5$ mm, $W1 = 20$ mm, $d1 = 0$, and $d2 = 0$).

5.15 GHz to 5.825 GHz is licensed to the WLAN, which partially overlaps with the operational band of the UWB communication systems. To reduce the mutual electromagnetic interference, the antennas with the band notches are usually employed in the UWB systems. Two symmetrical slots along with the microstrip line substitute the traditional C-shaped slot embedded in the patch to generate the desired notched band. Figure 3(a) depicts the geometry of the proposed antenna.

The shape of the slots embedded along with the feeding line looks like a flag, and these flag slots play a role as the stepped impedance resonator (SIR) [19–21]. The SIR is a resonator that is formed by joining two microstrip lines with the characteristic impedances Z_1 and Z_2 as well as the

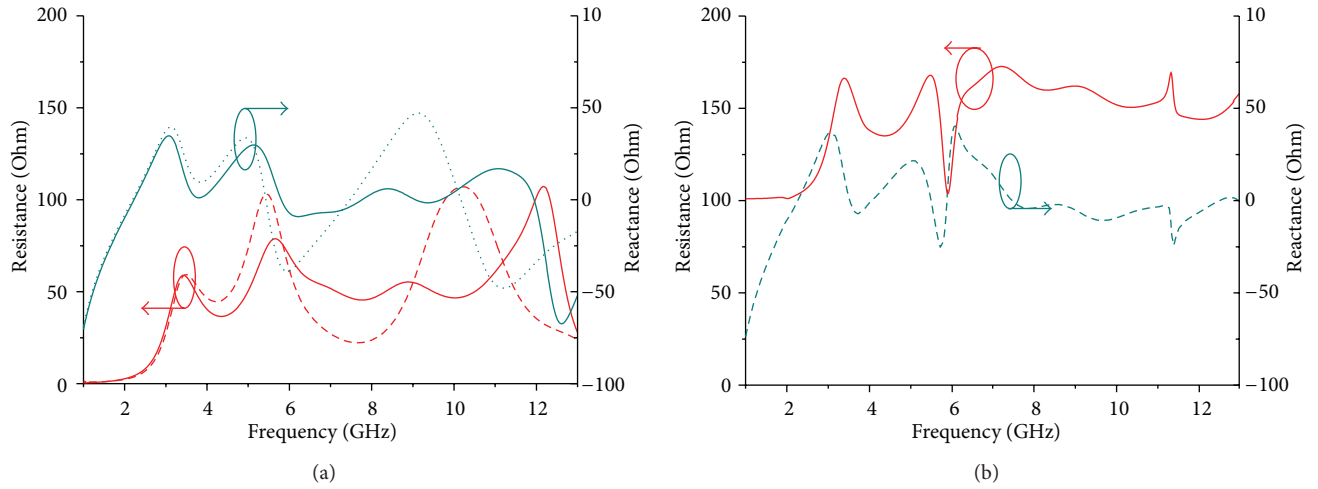

FIGURE 6: Frequency behavior of the real part of the antenna input impedance: (a) antenna without the band notch for different values of the parameter $W2$, solid line: $W2 = 13$ mm and dash line: $W2 = 16$ mm (other parameters: $G = 1$ mm, $L2 = 11$ mm, $Lg = 9$ mm, $L2 = 5$ mm, $W1 = 20$ mm, $d1 = 0$, and $d2 = 0$,) and (b) antenna with the band notch (other parameters: $Lv1 = 13.5$ mm, $Lv2 = 0$ mm, $Ln = 4$ mm, $S = 0.2$ mm, and $Ws = 1$ mm).

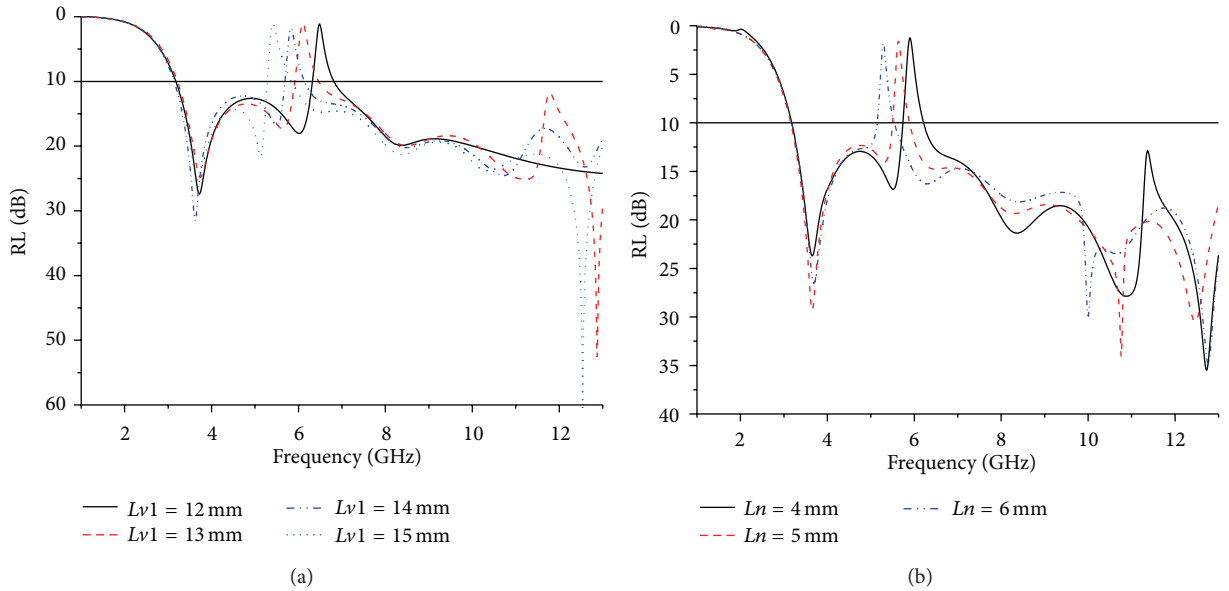

FIGURE 7: Band notch versus frequency (a) for different values of the parameter $Lv1$ (other parameters: $Lv2 = 0$ mm, $Ln = 4$ mm, $S = 0.2$ mm, and $Ws = 1$ mm) and (b) for different values of the parameter Ln (other parameters: $Lv2 = 0$ mm, $Lv1 = 13.5$ mm, $S = 0.2$ mm, and $Ws = 1$ mm).

electric lengths θ_1 and θ_2, respectively. Figure 3(b) shows that when Z_1 and Z_2 are equal the characteristic impedance of the resonator is uniform and accordingly a uniform impedance resonator (UIR) is obtained. In particular, the resonance condition of the SIR can be expressed as follows:

$$Z_2 - Z_1 \tan\theta_1 \tan\theta_2 = 0. \quad (1)$$

Thus,

$$\tan\theta_1 \tan\theta_2 = \frac{Z_2}{Z_1} = K, \quad (2)$$

where K denotes the impedance ratio. Compared to the UIR, the SIR can shorten the length of the resonator more effectively at the same resonant frequency by controlling the impedance ratio.

In this paper, two symmetrical slot SIRs, with the effective length of approximately half of the wavelength at the frequency of about 5.5 GHz, are adopted to construct the band-notched structure.

Near the antenna frequency notch, the dominant current around the notch structure flows in opposite directions as shown in Figure 3(c). Consequently, the radiated electric field in the far-field region becomes negligible. This behavior of the surface current explains the formation of the band notch in the frequency range from 5 GHz to 6 GHz.

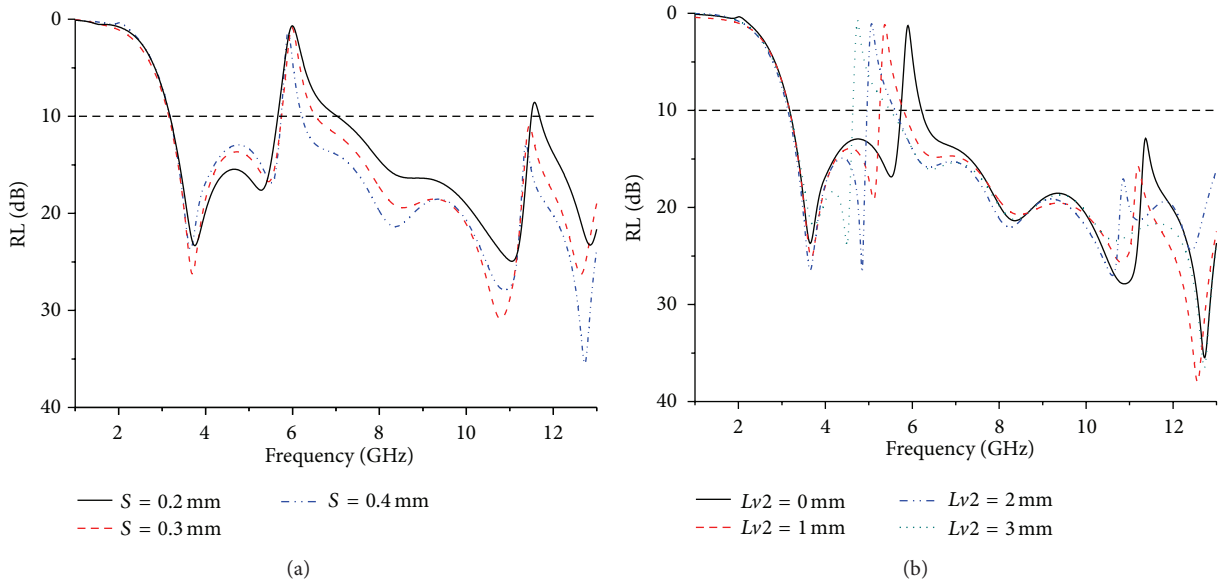

FIGURE 8: Band notch versus frequency (a) for different values of the parameter S (other parameters: $Lv2 = 0$ mm, $Ln = 4$ mm, $Lv1 = 0.2$ mm, and $Ws = 1$ mm) and (b) for different values of the parameter $Lv2$ (other parameters: $S = 0.2$ mm, $Lv1 = 13.5$ mm, $Ln = 4$ mm, and $Ws = 1$ mm).

3. Antenna Analysis and Design

3.1. Effects of the Geometrical Parameters on the Antenna Performance. The parameters of the two-step beveled antenna play a key role on the UWB impedance matching. These parameters are unconstrained variables except for *d1*, which is equal to half of the difference between *W1* and *W2*. In the following, we analyze the effects of the geometrical parameters on the antenna performance. In order to identify the role played by the geometrical parameters on the antenna performance, in the following the trends of the return loss versus the frequency, obtained by varying one parameter at a time while keeping all the others constant, are reported.

Figure 4 shows the effects of the geometrical parameters *L1* and *L2* on the antenna frequency band. From the numerical results reported in Figure 4, it is found that the lower and upper frequencies vary weakly as the parameter *L1* increases. When *L2* decreases, the lower and upper frequencies shift toward the higher frequencies simultaneously, and the bandwidth is broadened remarkably. This happens because the parameter *L1* is located in the region II that is far away from the edge of the truncated ground plane (see Figure 1) where the electric field is so weak that the parameter *L1* has a very small influence on the antenna impedance, while the region I is close to the ground plane and consequently the current distribution is stronger with respect to that excited in the region II. As the parameter *L2* decreases, the current path shortens, meaning that the reactive magnetic energy stored near the monopole reduces. Accordingly, the impedance matching at the upper frequency improves.

Since the region II weakly contributes to the antenna impedance matching, the analysis with respect to the parameter *W1* is not reported. As shown in Figure 5(a), with the decreasing of *W2*, the two-step structure is formed. The reactive electric energy excited close to the truncated ground plane neutralizes the reactive magnetic energy excited close to the monopole in the frequency range from 6 GHz to 12 GHz, thus maintaining the antenna reactance at values close to zero. The simulation results illustrated in Figure 6(a) reveal a suitable impedance matching.

The gap between the radiator and the ground, as denotedby *G*, is a crucial parameter that determines the electromagnetic coupling. A smaller gap means the tighter capacitive coupling, which further neutralizes the inductive reactance. Figure 5(b) illustrates a better impedance matching.

The length *Lg* of the truncated ground plane influences the lower frequency of the antenna. In particular, larger values of this parameter reduce this frequency even if this may lead to antennas of higher dimensions. In such a case, a compromise must be made. Considering the antenna size and performance, *Lg* is fixed at 9 mm. Eventually, the chamfered distance *d2* is optimized. All of the optimized parameters are listed in Table 1. The simulated return loss is shown in Figure 2 from which it can be found that the frequency band covers the range from 3 GHz to 13 GHz and meets the requirements of the UWB communication systems.

3.2. Effects of the Geometrical Parameters on the Band Notch. Figure 7 shows the effects of the parameters *Lv1* and *Ln* on the notch frequency which decreases as *Lv1* and *Ln* increase, even though the bandwidth of the stop band is almost constant at approximately 550 MHz, covering the frequency band from 5.18 GHz to 5.73 GHz when *Lv1* and *Ln* are equal to 15 mm and 4 mm, respectively. The sum of *Lv1* and *Ln* is approximately half of the wavelength of the notch frequency, which determines the resonant frequency of the slot resonator. When two symmetric slots are embedded along with the feed line, the radiation resistance is about zero Ohm in the vicinity of the notch frequency as shown

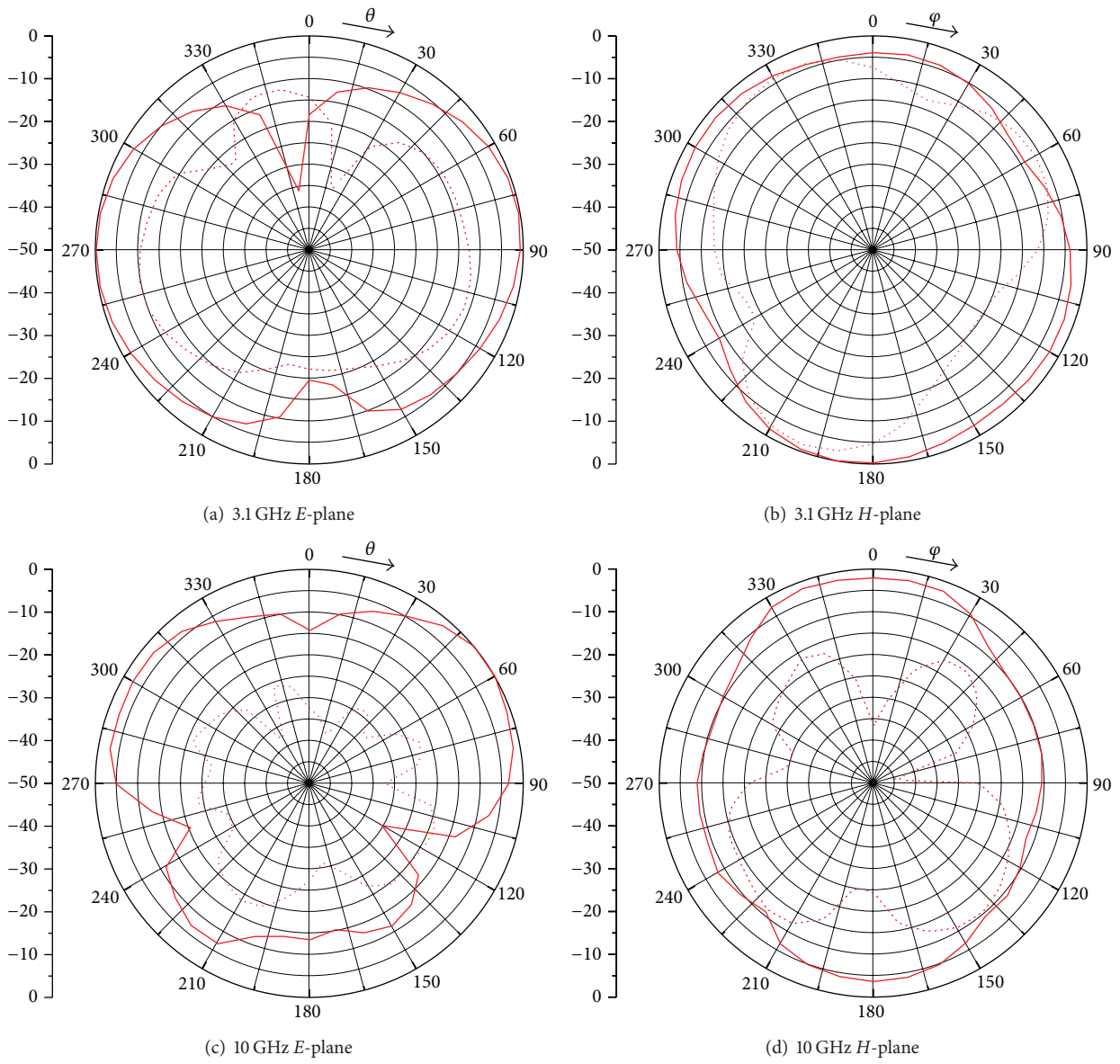

(a) 3.1 GHz *E*-plane

(b) 3.1 GHz *H*-plane

(c) 10 GHz *E*-plane

(d) 10 GHz *H*-plane

Figure 9: Normalized radiation patterns for the antenna without L-shaped slots loaded (solid line: copolar polarization and dash line: cross-polarization).

in Figure 6(b). Consequently, the radiation resistance is too small to enable an effective radiation process.

By changing the slot width, as denoted by *S*, the quality factor of the slot resonator can be adjusted. Figure 8(a) shows that the bandwidth of the stop band broadens significantly. When *S* is equal to 0.4 mm, the stop band covers the range from 5.7 GHz to 7 GHz. However, a spurious stop band is also formed. The integer multiples of the parasitic band are an inherent characteristic of UIR. Therefore, the location of the parasitic band can be changed against various impedance ratios of the SIR.

Figure 8(b) illustrates the effects of *Lv2* on the band notch. The impedance ratio of the SIR and the ratio of the second parasitic band to the main resonant frequency increase with the increasing of *Lv2*. The parasitic band is pushed outside 13 GHz when *Lv2* reaches 3 mm.

Table 2: Optimized parameters of the notch structure.

Parameters	Value (mm)	Parameters	Value (mm)
Lv1	13	*S*	0.4
Lv2	2.5	*Ln*	3.6

The effects of *Ws* on the band notch are negligible, and thus an exhaustive analysis is not indispensable. Table 2 reports the optimized parameters of the notch structure when *Ws is* fixed at 1 mm, and accordingly the notched band covers the range from 5.05 GHz to 6 GHz.

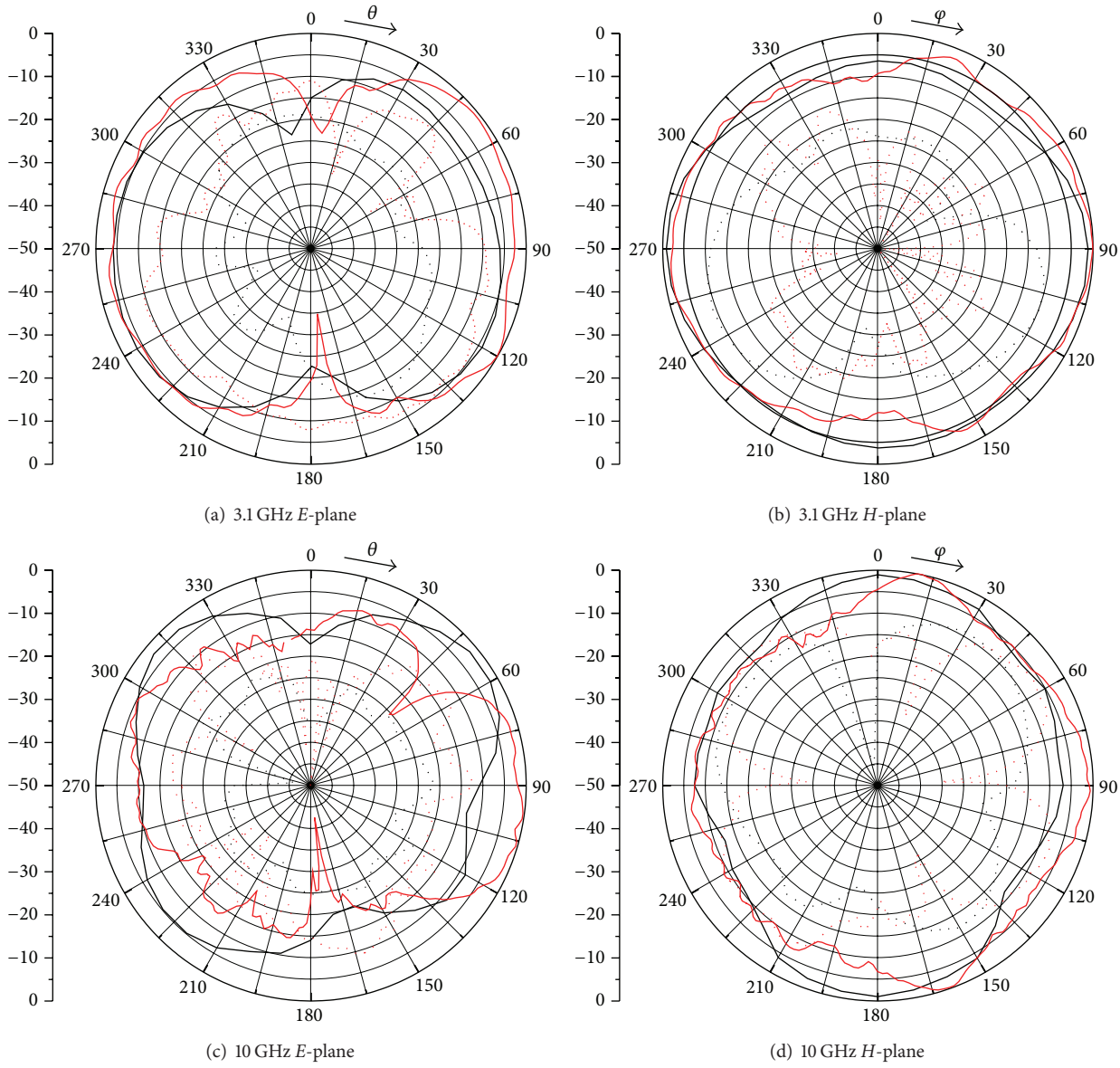

(a) 3.1 GHz E-plane

(b) 3.1 GHz H-plane

(c) 10 GHz E-plane

(d) 10 GHz H-plane

Figure 10: Normalized radiation patterns for the proposed antenna (red solid line: measured copolar polarization, black solid line: simulated copolar polarization, red dash line: measured cross-polarization, and black dash line: simulated cross-polarization).

3.3. Optimized Radiation Patterns. The radiation pattern is an important indicator of the antenna performance. Figure 9 illustrates the radiation patterns of the antenna depicted in Figure 1. The antenna radiation pattern significantly changes its shape at the upper frequency. In particular, it manifests an increasing cross-polarization effect. The radiation lobe tends to split in the E-plane (XOZ plane), while it loses its circular symmetry in the H-plane (XOY plane). This is due to the unequal surface current phase at a discrete frequency. At the lower frequency of 3.1 GHz, the length of the monopole equals approximately a half wavelength. Furthermore, the longitudinal current is in phase. But at 10 GHz, the physical length of the monopole exceeds a half wavelength, and also the out-phase longitudinal current contribution appears, which results in the null point in the far-field region.

The current distribution on the finite ground contributes to the radiation too. In order to improve the radiation patterns, two symmetrical L-shaped slots are embedded on the edge of the ground plane. Figure 3(a) shows the geometry of the proposed antenna with the band notch and optimized slot parameters.

Figure 10 shows the improved antenna radiation patterns. At the upper frequency of 10 GHz, the lobe of the radiation pattern in the E-plane splits barely, while the direction of the maximum radiation remains almost the same. The cross-polarization level is greater than 20 dB. The radiation pattern

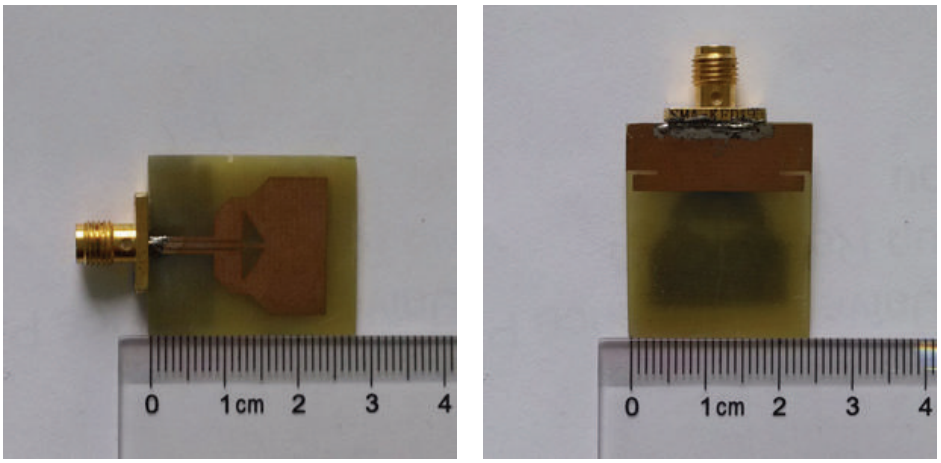

(a) (b)

Figure 11: Prototype of the proposed antenna: (a) top view and (b) bottom view.

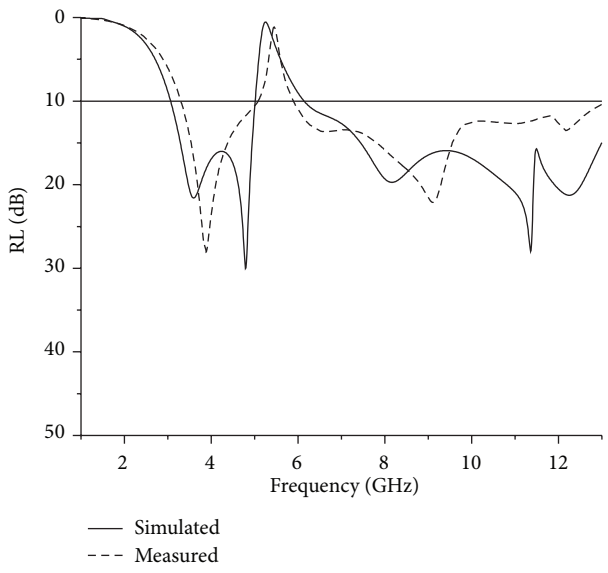

Figure 12: Comparison between the measured and simulated return losses.

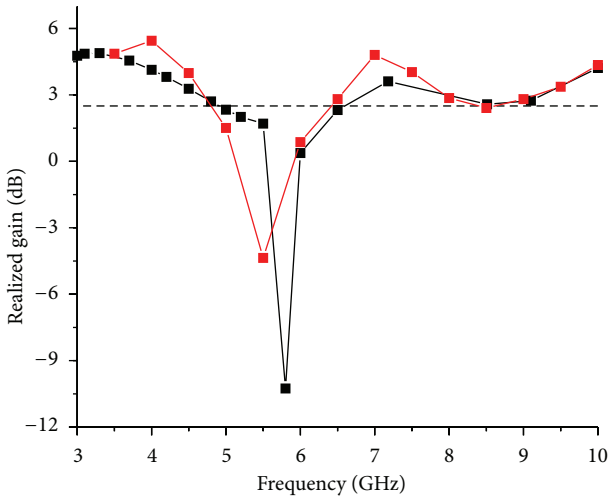

Figure 13: Peak gain of the proposed antenna (red solid line: measured gain and black solid line: simulated gain).

in the H-plane is nearly omnidirectional. Moreover, the cross-polarization level of the H-plane is also improved.

4. Fabrication and Measurement

The fabricated antenna, designed according to the methodology described above, is shown in Figure 11. The measurement results have been performed by using the Agilent N5232A vector network analyzer. The comparison between the experimental and simulation results in terms of the return loss is illustrated in Figure 12. From the experimental measurements, it is found that the band-notched filter covers the frequency range from 5.05 GHz up to 5.95 GHz. The measured notched band is less than the simulated one covering the range from 5.05 GHz to 6.05 GHz. The measured lower frequency with the return loss of 10 dB is 3.24 GHz, while that obtained via the numerical simulations is about 3.02 GHz. Such a deviation between the measurement and simulation results comes from the machining and permittivity tolerances, as well as from the irregular soldering whose perturbative effects are more evident at the higher frequencies. Finally, the measurement of the antenna peak gain is reported in Figure 13. This figure shows that the peak gain is about 2.5 dBi~3.6 dBi at the lower frequency, 3 dBi~4.5 dBi at the upper frequency, and below 0 dBi in the frequency band 5 GHz~6 GHz. The group delay properly quantifies the propagation properties of the so-called wave packet [2]. The signal integrity is confirmed by analyzing the relative group delay $\tau_{\text{grel}}(\omega)$, which is defined as

$$\tau_{\text{grel}}(\omega) = \tau_g(\omega) - \overline{\tau}_g, \tag{3}$$

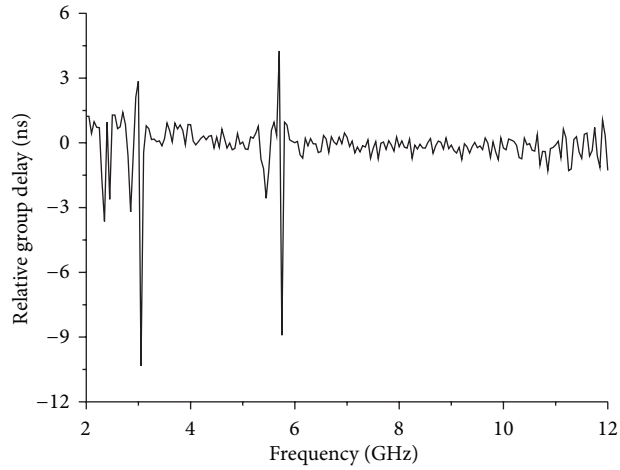

Figure 14: Frequency-domain behavior of the group delay.

where

$$\tau_g(\omega) = -\frac{d\phi(\omega)}{d\omega}, \quad (4)$$

denotes the group delay and $\phi(\omega)$ represents the phase of the radiated electromagnetic field. In (3), $\overline{\tau}_g$ denotes the mean value of the relative group delay that has been evaluated at a distance of 50 cm from the center of the proposed antenna along the X-axis. Figure 14 shows that the variations of the measured group delay are less than one nanosecond throughout the operational band expect in the band notch. These results indicate that the antenna has the good linear transmission performance and can be used in the multiband or impulse UWB radio applications.

5. Conclusion

A compact two-step beveled printed monopole antenna with the WLAN band-notch characteristic has been proposed in this paper. The effects of the geometrical parameters on the antenna performance have been investigated. A two-step structure has been utilized to broaden the bandwidth of the antenna impedance, while the slots embedded in the metal patch have been adopted to realize the notch band. By changing the parameters of the notch structure, the notch frequency and its bandwidth are controllable without perturbing the remaining part of the UWB band. In order to improve the shape of the radiation patterns at the upper frequency, two L-shaped slots have been integrated on the edge of the ground plane. Since the proposed antenna presents a compact structure (the overall size of the antenna is 24 mm × 28 mm) and a stable radiation pattern, it is able to be effectively utilized in the UWB radio communication systems.

Conflict of Interests

The authors declare that there is no conflict of interests regarding the publication of this paper.

Acknowledgment

The authors would like to acknowledge National Natural Science Foundation of China (61172086) for providing the financial support for this work.

References

[1] "First Report and order in the Matter of Revision of Part 15 of the Commission's Rules Regarding Ultra-Wideband Transmission System from 3.1 to 10.6 GHz.," in *FCC*, pp. 98–153, ETDocket, FCC, Washington, DC, USA, 2002.

[2] G. Cappelletti, D. Caratelli, R. Cicchetti, and M. Simeoni, "A low-profile printed drop-shaped dipole antenna for wide-band wireless applications," *IEEE Transactions on Antennas and Propagation*, vol. 59, no. 10, pp. 3526–3535, 2011.

[3] G. Quintero and A. K. Skrivervik, "Analysis of planar UWB elliptical dipoles fed by a coplanar stripline," in *Proceedings of the IEEE International Conference on Ultra-Wideband (ICUWB '08)*, pp. 113–116, September 2008.

[4] G. Teni, N. Zhang, J. Qiu, and P. Zhang, "Research on a novel miniaturized antipodal Vivaldi antenna with improved radiation," *IEEE Antennas and Wireless Propagation Letters*, vol. 12, pp. 417–420, 2013.

[5] D. Guha and Y. M. M. Antar, , *Microstrip and Printed Antennas*, Wiley, New York, NY, USA, 2011.

[6] C. Abdelhalim and D. Farid, "A compact planar UWB antenna with triple controllable band-Notched characteristics," *International Journal of Antennas and Propagation*, vol. 2014, Article ID 848062, 9 pages, 2014.

[7] L. Liu, S. W. Cheung, R. Azim, and M. T. Islam, "A compact circular-ring antenna for ultra-wideband applications," *Microwave and Optical Technology Letters*, vol. 53, no. 10, pp. 2283–2288, 2011.

[8] R. Azim, M. T. Islam, and N. Misran, "Printed circular disc compact planar antenna for UWB applications," *Telecommunication Systems*, vol. 52, no. 2, pp. 1171–1177, 2013.

[9] M. Ojaroudi, S. Yazdanifard, N. Ojaroudi, and R. A. Sadeghzadeh, "Band-notched small square-ring antenna with a pair of T-shaped strips protruded inside the square ring for UWB applications," *IEEE Antennas and Wireless Propagation Letters*, vol. 10, pp. 227–230, 2011.

[10] M. Ojaroudi, G. Ghanbari, N. Ojaroudi, and C. Ghobadi, "Small square monopole antenna for UWB applications with variable frequency band-notch function," *IEEE Antennas and Wireless Propagation Letters*, vol. 8, pp. 1061–1064, 2009.

[11] A. Nouri and G. R. Dadashzadeh, "A compact UWB band-notched printed monopole antenna with defected ground structure," *IEEE Antennas and Wireless Propagation Letters*, vol. 10, pp. 1178–1181, 2011.

[12] R. Shi, X. Xu, J. Dong et al., "Design and analysis of a novel dual band-notched UWB antenna," *International Journal of Antennas and Propagation*, vol. 2014, Article ID 531959, 11 pages, 2014.

[13] R. Azim and M. T. Islam, "Compact planar UWB antenna with band notch characteristics for WLAN and DSRC," *Progress in Electromagnetics Research*, vol. 133, pp. 391–406, 2013.

[14] A. A. Gheethan and D. E. Anagnostou, "Dual band-reject UWB antenna with sharp rejection of narrow and closely-spaced bands," *IEEE Transactions on Antennas and Propagation*, vol. 60, no. 4, pp. 2071–2076, 2012.

[15] M. T. Islam, R. Azim, and A. T. Mobashsher, "Triple band-notched planar UWB antenna using parasitic strips," *Progress in Electromagnetics Research*, vol. 129, pp. 161–179, 2012.

[16] S. Barbarino and F. Consoli, "UWB circular slot antenna provided with an inverted-L notch filter for the 5 GHz WLAN band," *Progress in Electromagnetics Research*, vol. 104, pp. 1–13, 2010.

[17] J. X. Liu, W. Y. Yin, and S. L. He, "A new defected ground structure and its application for miniaturized switchable antenna," *Progress in Electromagnetics Research*, vol. 107, pp. 115–128, 2010.

[18] M. Yazdi and N. Komjani, "Design of a band-notched UWB monopole antenna by means of an EBG structure," *IEEE Antennas and Wireless Propagation Letters*, vol. 10, pp. 170–173, 2011.

[19] M. Makimoto and S. Yamashita, *Microwave Resonators and Filters for Wireless Communication: Theory, Design and Application*, Springer, New York, NY, USA, 2001.

[20] S. W. Chen, D. Y. Wang, and W. H. Tu, "Dual-band/tri-band/broadband CPW-fed stepped-impedance slot dipole antennas," *IEEE Transactions on Antennas and Propagation*, vol. 62, no. 1, pp. 485–490, 2014.

[21] R. Y. Fang, C. F. Liu, and C. L. Wang, "Compact and broadband CB-CPW-to-SIW transition using stepped-impedance resonator with 90°-bent slot," *IEEE Transactions on Components, Packaging and Manufacturing Technology*, vol. 3, no. 2, pp. 247–252, 2013.

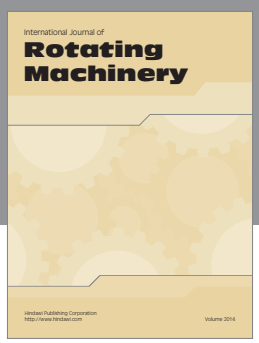

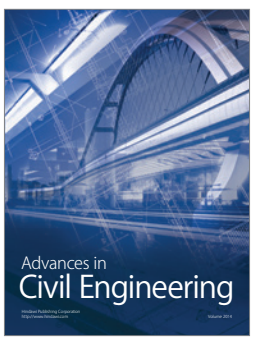

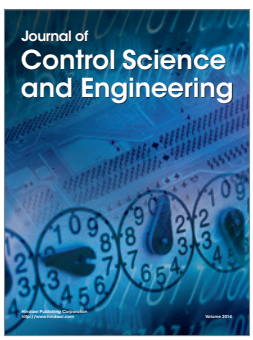

Hindawi
Submit your manuscripts at
http://www.hindawi.com